INTERNATIONAL JOURNAL FOR NUMERICAL METHODS IN FLUIDS
Int. J. Numer. Meth. Fluids 2009; **61**:165–184
Published online 17 November 2008 in Wiley InterScience (www.interscience.wiley.com). DOI: 10.1002/fld.1954

A meshless numerical wave tank for simulation of nonlinear irregular waves in shallow water

Long-Fei Xiao*,†,‡, Jian-Min Yang, Tao Peng and Jun Li

State Key Lab of Ocean Engineering, Shanghai Jiao Tong University, Shanghai 200030, China

SUMMARY

Time domain simulation of the interaction between offshore structures and irregular waves in shallow water becomes a focus due to significant increase of liquefied natural gas (LNG) terminals. To obtain the time series of irregular waves in shallow water, a numerical wave tank is developed by using the meshless method for simulation of 2D nonlinear irregular waves propagating from deep water to shallow water. Using the fundamental solution of Laplace equation as the radial basis function (RBF) and locating the source points outside the computational domain, the problem of water wave propagation is solved by collocation of boundary points. In order to improve the computation stability, both the incident wave elevation and velocity potential are applied to the wave generation. A sponge damping layer combined with the Sommerfeld radiation condition is used on the radiation boundary. The present model is applied to simulate the propagation of regular and irregular waves. The numerical results are validated by analytical solutions and experimental data and good agreements are observed. Copyright © 2008 John Wiley & Sons, Ltd.

Received 20 January 2008; Revised 2 September 2008; Accepted 23 September 2008

KEY WORDS: meshless method; numerical wave tank; irregular wave; shallow water

1. INTRODUCTION

In recent years, the worldwide booming liquefied natural gas (LNG) market leads to significant increase of offshore LNG receiving terminals. In general, those facilities are designed as floating bodies and located as close to the shore as possible in order to reduce the cost of the necessary

*Correspondence to: Long-Fei Xiao, State Key Lab of Ocean Engineering, Shanghai Jiao Tong University, Shanghai 200030, China.
†E-mail: xiaolf@sjtu.edu.cn
‡Associate Professor.

Contract/grant sponsor: National High Technology and Development Program of China; contract/grant number: 2006AA09A107
Contract/grant sponsor: Shanghai Natural Science Foundation; contract/grant number: 07ZR14048

Copyright © 2008 John Wiley & Sons, Ltd.

pipelines. Therefore, they will likely be located in shallow water. As a result, safety problems associated with shallow water hydrodynamics of floating bodies should be paid attention to, especially the interaction between the floating bodies and the irregular waves in shallow water. As the input for time domain simulation of the interaction, time series of irregular waves should be known first and obtained numerically or experimentally.

Numerical simulation of surface gravity water waves is an important topic in the field of coastal and ocean engineering. Along with the continuous increase of computer technique and power, many different types of numerical wave tanks (NWT) on the basis of different numerical methods and numerical techniques have been developed to simulate the propagation of water waves in the past decades [1–10]. Almost all the traditional numerical methods, such as the finite difference method (FDM) [2, 3], the finite element method [4, 5], the boundary element method (BEM) [6–8] and the volume of fluid (VOF) [9, 10], have been applied to develop the NWT.

By solving the Navier–Stokes equation, the VOF-type NWT can be used to simulate the overturning waves, the breaking waves, the green water on offshore structures, etc. However, the most severe limitation of VOF-type NWT is the huge time consumption, which is almost 50 times that of the BEM-type NWT for the same simulation [11]. The BEM is efficient in solving the Laplace equation and the main advantage lies in having only to discretize the boundary of fluid domain, which provides a simpler way of tracking the motion of water nodes on the free surface and at the same time reduces one dimension of the problem. It is a very accurate and fast method for solving the hydrodynamic problem under the assumptions of inviscous flow, irrotational flow and incompressibility. Thus, the BEM-type NWT is also very popular for simulating the propagation of water waves on condition that the viscosity is not important. By the mixed Eulerian–Lagrangian (MEL) approach [12], the velocity potential of the boundary value problem can be solved at each time step and the particle trajectories along with the nonlinear boundary conditions on the free surface can be calculated in the time domain. However, boundary integral equations with existence of singularities mean that a time-consuming numerical integration procedure should be conducted [13]. Furthermore, dense matrices will be produced and solving the linear algebraic system would take much time, although some efficient numerical techniques can be utilized to speed up computation [14–16]. Another alternative model is based on the shallow water equations by using FDM [17, 18]. It uses the assumption of hydrostatic pressure and the applicability of water depth is limited.

To avoid the shortcomings of numerical methods based on mesh like the BEM, many meshless methods have been proposed, and remarkable progress has been achieved over the past few years [19–21]. A common feature of the meshless method is that neither domain nor surface meshing is required during the solution of boundary and initial value problems. Thus, these meshless methods have been successfully applied to a large variety of problems in many fields of science and technology [22]. Among these various meshless methods, the purest may be the one based on radial basis functions (RBF), which state the relationship between the two-point distances [23, 24]. In its applications to solving boundary problems, the fundamental solution of the linear operator is usually chosen as the RBF [25], which will automatically satisfy the governing equation except at the center of RBF (source point). Furthermore, if all the source points are set outside the computational domain, there will be no singularity in the computational domain at all and the governing equation is satisfied automatically. The remaining task is only to satisfy the boundary conditions. By collocating points on the boundary, the boundary conditions can be solved directly without singular numerical integrations and the solution procedure is easier to be implemented and the computational time can be economized.

Copyright © 2008 John Wiley & Sons, Ltd.

DOI: 10.1002/fld

The boundary meshless method based on the RBF is also introduced recently to establish a NWT and simulate the propagation of nonlinear regular waves [26]. Numerical simulation of periodic finite-amplitude waves and monochromatic waves passing over a submerged obstacle is conducted and good agreements are observed as compared with experimental data and other numerical models. However, for the simulation of irregular waves, it is necessary to improve the meshless NWT further. The difficulties mainly exist in the treatment of space derivatives, the wave generation and the wave absorption method. First, the calculation of space derivatives is the substantial disadvantage of the meshless method since it easily causes instability of the computation [24]. Second, the piston-type and other kinds of wave generators also utilize the normal velocities of the incident waves and then also easily bring about numerical instability. Finally, it is not effective that only the radiation condition is used in the meshless NWT for simulation of irregular waves that consist of regular wave components with different wavelengths.

In the present work, a new meshless NWT is developed with further improvements for simulating the propagation of 2D nonlinear irregular water waves. In order to improve the stability of numerical simulation, the incident wave elevation and velocity potential are applied to the wave generation simultaneously. A sponge damping layer for wave absorption combined with the Sommerfeld radiation condition is used on the radiation boundary. The present model is applied to simulate the propagation of irregular wave profiles from deep water to shallow water. The numerical results are validated by wave simulation experiments conducted in the physical ocean engineering basin. Good agreements indicate that the meshless numerical algorithm is valid for the simulation of irregular waves.

2. GOVERNING EQUATION AND BOUNDARY CONDITIONS

The problem of the free surface water wave propagating in a 2D wave tank is shown in Figure 1. Here, Ω denotes the computational fluid domain, while Γ_F, Γ_I, Γ_B and Γ_R denote the instantaneous free surface boundary, the incident boundary, the bottom boundary and the radiation boundary, respectively. A Cartesian coordinate system oxz is employed as shown in Figure 1 and the plane of $z=0$ coincides with the undisturbed still water level. The x-axis is directed horizontally along the wave propagation and the z-axis is directed vertically upward.

The fluid is assumed to be inviscid and incompressible and the flow is irrotational, so that the fluid domain can be described in terms of a velocity potential that satisfies Laplace equation

$$\nabla^2\phi(x,z,t)=0 \quad \text{in } \Omega \tag{1}$$

where $\phi(x,z,t)$ is the velocity potential.

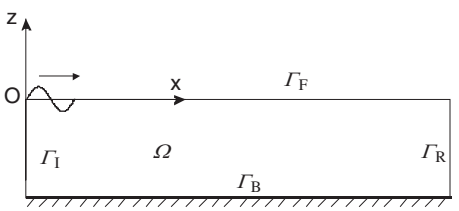

Figure 1. Sketch of a 2D numerical wave tank.

Copyright © 2008 John Wiley & Sons, Ltd.

DOI: 10.1002/fld

Equation (1) is an elliptic-type equation that requires all the values on the boundaries to be defined. The boundary conditions for simulating fully nonlinear water waves can be described as

$$\phi = \phi(0, z, t) \quad \text{on } \Gamma_{\mathrm{I}} \tag{2}$$

$$\left.\frac{\partial \phi}{\partial z}\right|_{z=-h} = -\left.\frac{\partial \phi}{\partial x}\right|_{z=-h} \frac{\mathrm{d}h}{\mathrm{d}x} \quad \text{on } \Gamma_{\mathrm{B}} \tag{3}$$

$$\frac{\partial \phi}{\partial t} + c\frac{\partial \phi}{\partial n} = 0 \quad \text{on } \Gamma_{\mathrm{R}} \tag{4}$$

$$\frac{\partial \phi}{\partial z} = \frac{\partial \eta}{\partial t} + \frac{\partial \eta}{\partial x}\frac{\partial \phi}{\partial x} \quad \text{on } \Gamma_{\mathrm{F}} \tag{5}$$

$$\frac{\partial \phi}{\partial t} + g\eta + \frac{1}{2}(\nabla \phi)^2 = 0 \quad \text{on } \Gamma_{\mathrm{F}} \tag{6}$$

where $\eta(x, t)$ is the free surface displacement, $h(x)$ is the water depth, c is the wave speed, $\vec{n}$ is the unit outward normal vector on the boundary and g is the acceleration of gravity. Equation (4) denotes the radiation boundary condition, which means waves are always outgoing. Equations (5) and (6) are called the kinematic and dynamic free surface boundary conditions, respectively.

The initial conditions can be written as

$$\eta|_{t=0} = 0 \quad \text{on } \Gamma_{\mathrm{F}} \tag{7}$$

$$\phi|_{t=0} = 0 \quad \text{on } \Gamma_{\mathrm{F}} \text{ and } \Gamma_{\mathrm{R}} \tag{8}$$

To solve the hydrodynamic problem described as above Equations (1)–(8), the MEL approach is applied. The movement of fluid particles on the instantaneous-free surface is tracked in the Lagrangian reference frame and the boundary conditions are solved in the Eulerian reference frame at each time step.

3. METHOD OF FUNDAMENTAL SOLUTIONS

3.1. Meshless numerical method

In the MEL approach, the time-dependent velocity potential and wave elevation in Equations (1)–(6) will be computed through a time-stepping integration procedure described in Section 3.4. While at each time step, the boundary conditions will be solved to obtain the fluid velocity on the free surface. In the meshless method based on collocation with RBF, the velocity potential at each time step is assumed as the linear combination of N RBFs, taking nth time step as example [26]

$$\phi^{(n)}(x, z) = \sum_{i=1}^{N} \alpha_i^{(n)} q_i(x, z) \tag{9}$$

where $q_i(x, z)$ is the RBF whose center (also named source point) is at (x_i, z_i), and $\alpha_i^{(n)}$ is its weight, which is a function of time like the velocity potential. The type of RBF is chosen as the fundamental solution of a 2D Laplace operator

$$q_i(x, z) = \ln r_i \tag{10}$$

Copyright © 2008 John Wiley & Sons, Ltd.

DOI: 10.1002/fld

where $r_i = \sqrt{(x-x_i)^2+(z-z_i)^2}$ is the distance between any field point (x, z) in the computational fluid domain and the source point (x_i, z_i). If all the source points are laid outside the fluid domain, the solution form will satisfy the governing equation automatically.

Based on the solution form described in Equation (9), the partial derivatives of the velocity potential can be written as

$$\left(\frac{\partial \phi}{\partial x}\right)^{(n)} = \sum_{i=1}^{N} \alpha_i^{(n)} \frac{x-x_i}{r_i^2} \tag{11}$$

$$\left(\frac{\partial \phi}{\partial z}\right)^{(n)} = \sum_{i=1}^{N} \alpha_i^{(n)} \frac{z-z_i}{r_i^2} \tag{12}$$

At each time step, the wave elevations and the velocity potentials on Γ_I and Γ_F , and the normal velocities on Γ_B and Γ_R are known. Therefore, the solution $\alpha_i^{(n)}$ of all the source points can be obtained by solving the boundary equations. The boundary conditions at the free surface can be applied directly by using Equation (9) since the velocity potential is obtained by the $(n-1)$th time step computation. This approach is rather straightforward without any iteration in the procedure of forming linear algebraic equations for solving $\alpha_i^{(n)}$. Unlike the traditional BEM, this approach is more effective since no time domain integrations are needed for generating the coefficient matrix of the linear algebraic equations.

3.2. Numerical wave generator

In the simulation of NWT, the fluid motion is generated either by a prescribed wave-maker motion similar to the physical wave generator, or by specifying the wave elevations and the normal velocities analytically according to a chosen wave theory on the incident boundary. In terms of different techniques, many numerical wave generators have been developed. For simulation of fully nonlinear waves in an NWT, the wave generator based on analytical specifications is relatively simpler to implement because it does not involve constant updating of the fluid domain due to the wave-maker motions [27]. However, it may cause numerical instability in the simulation by using the meshless method, since derivative computations should be conducted on the velocity potentials on the incident boundary. In this study, a new wave generation technique is introduced by specifying both the wave elevations and the velocity potentials on the incident boundary based on the theoretical wave solutions, as described in Equation (2).

The incident waves on the incident boundary are increased gradually by using a ramping function, which smoothly approaches unity from zero as the simulation proceeds. The ramping function is to reduce the transient effect so as to make the numerical simulation stable and reach the steady state properly. In the present simulation, the following ramping function is utilized:

$$R_m(t) = \begin{cases} \dfrac{1}{2}\left(1-\cos\dfrac{\pi t}{T_m}\right), & t \leqslant T_m \\ 1, & t > T_m \end{cases} \tag{13}$$

where T_m is the modulation time, in which the incident waves are ramped. It is usually set as several times of the wave period.

Copyright © 2008 John Wiley & Sons, Ltd.

DOI: 10.1002/fld

3.3. Numerical wave absorption

In this study, both a damping layer and the Sommerfeld radiation condition given in Equation (4) are used to prevent wave reflection. The former absorbs the wave energy gradually in the direction of water wave propagation and the latter keeps the transmitted wave outgoing. For the damping layer scheme, extra terms are added to both the kinematic and dynamic-free surface boundary conditions given in Equations (5) and (6) as follows:

$$\frac{\partial \eta}{\partial t} = \frac{\partial \phi}{\partial z} - \frac{\partial \eta}{\partial x}\frac{\partial \phi}{\partial x} - v(x)\eta \tag{14}$$

$$\frac{\partial \phi}{\partial t} = -g\eta - \frac{1}{2}(\nabla\phi)^2 - v(x)\phi \tag{15}$$

where $v(x)$ is a tunable damping factor inside the damping layer to prevent the wave reflection and usually written in a quadratic function form. That is

$$v(x) = \begin{cases} \alpha\omega\left[\dfrac{x-(L-\beta\lambda)}{\beta\lambda}\right]^2, & L-\beta\lambda \leqslant x \leqslant L \\ 0, & x < L-\beta\lambda \end{cases} \tag{16}$$

where L is the total length of the NWT, λ is the wavelength, α is the tuning factor and $\beta\lambda$ denotes the length of the damping layer, respectively. It is found that the reflection coefficient is less than 2% [28, 29] when the length of the damping layer is set to be at least one wavelength ($\beta \geqslant 1.0$) by using $\alpha = 1.0$.

The Sommerfeld radiation condition given by Equation (4) can be rewritten as [26]

$$\phi^{(n+1)} + \frac{c\Delta t}{2}\left(\frac{\partial \phi}{\partial x}\right)^{(n+1)} = \phi^{(n)} - \frac{c\Delta t}{2}\left(\frac{\partial \phi}{\partial x}\right)^{(n)} \tag{17}$$

where the superscripts (n) and $(n+1)$ denote the time steps.

3.4. Time-stepping integration scheme

In the MEL approach, a time-stepping integration procedure must be employed to obtain the values of wave elevations and velocity potentials on the instantaneous-free surface. After solving the boundary conditions by using the meshless method mentioned above and obtaining the fluid velocity on the free surface at each time step, the free surface boundary conditions with the damping layer given by Equations (14) and (15) can be treated as ordinary differential equations to be marched in time. If there is no wave breaking in the wave propagation, the wave elevation can be assumed to be single valued and the collocation points on the instantaneous free surface can be allowed to move vertically only (semi-Lagrangian). Therefore, the wave elevations and the velocity potentials on the instantaneous free surface can be expressed as a second-order Taylor series [30]

$$\eta(x, t+\Delta t) = \eta(x,t) + \frac{\Delta t}{2}\left(3\frac{\partial \eta}{\partial t}\bigg|_t - \frac{\partial \eta}{\partial t}\bigg|_{t-\Delta t}\right) \tag{18}$$

$$\phi(x, z+\Delta z, t+\Delta t) = \phi(x,z,t) + \frac{\Delta t}{2}\left(3\frac{\partial \phi}{\partial t}\bigg|_t - \frac{\partial \phi}{\partial t}\bigg|_{t-\Delta t}\right) + \frac{\Delta z}{2}\left(5\frac{\partial \phi}{\partial z}\bigg|_t - 3\frac{\partial \phi}{\partial z}\bigg|_{t-\Delta t}\right) \tag{19}$$

Copyright © 2008 John Wiley & Sons, Ltd.

DOI: 10.1002/fld

where Δt is the time step and $\Delta z = \eta(x, t+\Delta t) - \eta(x, t)$ is the change of the wave elevation calculated by Equation (18). At the beginning of time-stepping integration procedure, a simplified first-order form is utilized as follows:

$$\eta|_{t=\Delta t} = \eta|_{t=0} + \Delta t \left.\frac{\partial \eta}{\partial t}\right|_{t=0} \tag{20}$$

$$\phi|_{t=\Delta t} = \phi|_{t=0} + \Delta t \left.\frac{\partial \phi}{\partial t}\right|_{t=0} + \Delta z \left.\frac{\partial \phi}{\partial z}\right|_{t=0} \tag{21}$$

3.5. Numerical difference and smoothing scheme

In the fully nonlinear free surface boundary conditions given by Equations (5) and (6), there are space derivative terms on the wave elevation and the velocity potential. To avoid instability, a seven-point difference scheme is applied to calculate the derivatives by x instead of Equation (11), as shown as follows:

$$\left(\frac{\partial \eta}{\partial x}\right)_i = \frac{1}{60\Delta x}[-45(\eta_{i-1} - \eta_{i+1}) + 9(\eta_{i-2} - \eta_{i+2}) - (\eta_{i-3} - \eta_{i+3})] \tag{22}$$

$$\left(\frac{\partial \phi}{\partial x}\right)_i = \frac{1}{60\Delta x}[-45(\phi_{i-1} - \phi_{i+1}) + 9(\phi_{i-2} - \phi_{i+2}) - (\phi_{i-3} - \phi_{i+3})] \tag{23}$$

Furthermore, to maintain numerical accuracy and avoid instability, a five-point smoothing scheme is applied to smooth the free surface profile and the velocity potential during time-stepping integration procedure, as shown as follows:

$$\bar{\eta}_i = \frac{1}{35}[17\eta_i + 12(\eta_{i-1} + \eta_{i+1}) - 3(\eta_{i-2} + \eta_{i+2})] \tag{24}$$

$$\bar{\phi}_i = \frac{1}{35}[17\phi_i + 12(\phi_{i-1} + \phi_{i+1}) - 3(\phi_{i-2} + \phi_{i+2})] \tag{25}$$

4. CONFIGURATION OF MESHLESS NWT

As mentioned above, the numerical wave generator based on analytical specifications of incident wave properties is relatively simpler for a fully nonlinear NWT. For regular waves or deep water irregular waves, it is feasible since both the wave elevation and the velocity potentials can be evaluated analytically. However, for incident irregular waves in shallow water, it is difficult to specify the incident boundary conditions since the approximation of linear combination of regular wave components is not applicable. In this study, a new form of nonlinear NWT is established including a deep water region, a transition region and a shallow water region. The incident boundary condition in deep water is specified by using the approximation of linear combination. Then, meshless numerical simulation is conducted on the wave propagation from the deep water region to the shallow water region and the time series of irregular waves in shallow water can be obtained.

Copyright © 2008 John Wiley & Sons, Ltd.

DOI: 10.1002/fld

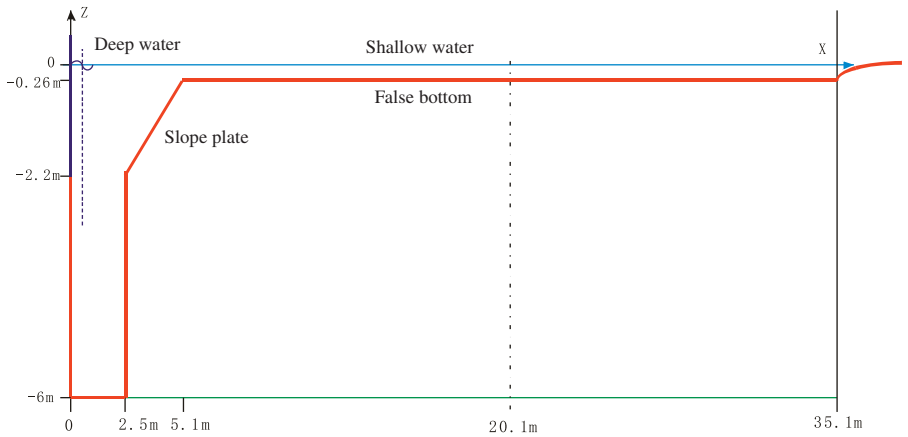

Figure 2. Profile of the ocean engineering basin during wave simulation in shallow water.

4.1. A new form NWT

The physical ocean engineering basin in Shanghai Jiao Tong University is capable of varying the water depth randomly between 0 and 5 m by adjusting a large false bottom up and down. The profile of the basin is shown in Figure 2 during simulation of shallow water depth.

At one side of the basin, a dual-flap-type hydraulic wave generator is equipped to generate long-crest regular and irregular waves. Within a range of 2.5 m in front of the wave generator, the water depth is constant at 6 m where deep water waves exist. From $X=2.5$ to $X=5.1$ m, there is a guidance slope plate with one fixed end at water depth of 2.2 m and another free end to be adjusted up and down. During the simulation of shallow water depth, the slope plate will be used as a smooth transition bottom from deep water to shallow water. From $X=5.1$ to $X=35.1$ m, there is a large region with uniform water depth adjusted freely by the false bottom. At the end of the basin, a slope beach is located to absorb the wave energy and avoid the wave reflection.

Since the water depth within an area from $X=0$ to $X=2.5$ m is relatively deep, the linear theory can be applied to specify the irregular wave properties. If the numerical incident boundary is located in this deep water region, the wave elevation and the velocity potentials of incident irregular waves can be specified by using the conventional approximation of linear combination of regular wave components. Thus, the incident boundary condition is known and the meshless numerical simulation of irregular wave propagation can be realized. Based on this concept, a new form NWT can be configured as Figure 3 with the similar profile as the physical ocean engineering basin. The deep water region is chosen less deep in order to simplify the numerical simulation with negligible effect on the wave generation and propagation.

In the NWT, the total length is selected as 20 m and the lengths of the deep water region, the slope bottom and the uniform shallow water region are 2.0, 2.6 and 15.4 m, respectively. A damping layer is located in the shallow water region and near the radiation boundary. The water depth h_R in the shallow water region can be selected randomly. The water depth of the deep water region is selected as a constant value of 2.2 m, equivalent to the water depth of the fixed end of the slope plate in the physical wave basin. At several positions in the NWT, numerical wave probes are placed to record the wave elevations. Especially in the numerical wave probe at $x=15$ m, the

Copyright © 2008 John Wiley & Sons, Ltd.

DOI: 10.1002/fld

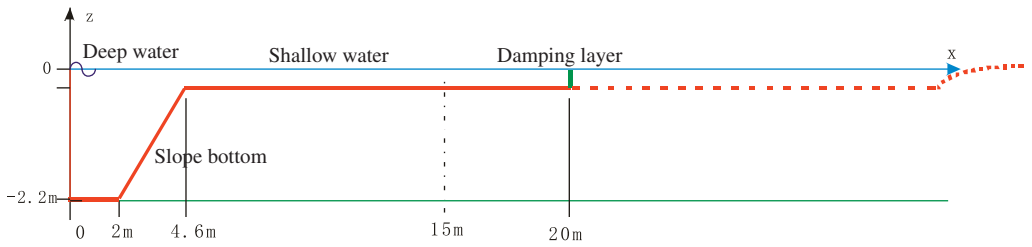

Figure 3. Sketch of the 2D NWT for simulating shallow water waves.

recorded wave elevations will be analyzed as the numerical results of the meshless simulation of irregular waves.

4.2. *Numerical wave generator for incident irregular waves*

A numerical wave generator for incident irregular waves can be established similar to the wave generation method in the physical wave basin [31]. In the deep water region, the linear theory can be adopted and the long-crested irregular wave elevation propagating along the positive x-axis can be written as the sum of a large number of regular wave components, i.e.

$$\eta(t)=\sum_{l=1}^{M}\sqrt{2S(\omega_l)\Delta\omega_l}\cos(\omega_l t+\varepsilon_l) \tag{26}$$

where $S(\omega_l)$ is the wave spectrum value at the circular frequency defined as ω_l, $\Delta\omega_l$ is a constant difference between successive wave frequencies, ε_l is the random wave phase that is uniformly distributed between 0 and 2π and constant with time. The random phases of all the wave components can be generated automatically by using the well-known random function and determined by the random seed as input.

In the NWT, the time series of the wave elevation on the incident boundary can be determined by Equation (26) if the irregular wave spectrum is known. Besides, the wave velocity potentials on the incident boundary can be determined similarly by using the linear combination of the wave velocity potentials of regular wave components. The formula can be written as

$$\phi(0,z,t)=\sum_{l=1}^{M}\frac{\sqrt{2S(\omega_l)\Delta\omega_l}\,g}{\omega_l}\frac{\cosh k_l(z+h)}{\cosh k_l h}\sin(\omega_l t+\varepsilon_l) \tag{27}$$

where $z=-h\sim\eta(t)$ is the vertical coordinate from the bottom to the wave elevation on the incident boundary.

4.3. *Iterated modification of wave spectrum*

After numerical simulation, the wave spectrum can be obtained by spectral analysis of the time series of wave elevation recorded by the wave probe located at $x=15.0$ m. Comparisons can be made between the numerical and target wave spectrums and conclusions can be drawn whether the simulation of the irregular wave is acceptable. Similar to the wave modeling procedure in the physical wave basin, generally it cannot be achieved by only one simulation. During the nonlinear wave propagation of the irregular wave, the wave profile is distorted continuously, especially in the

Copyright © 2008 John Wiley & Sons, Ltd.

DOI: 10.1002/fld

regions of the slope bottom and the shallow water. Thus, iterated modification procedure should be done and the driven spectrum should be updated by comparing the recorded wave spectrum and the target one. The updated wave generation and wave simulation should be conducted several times to obtain satisfied irregular waves finally.

In the wave simulation, the target wave spectrum $S_T(\omega)$ is utilized as the first-driven wave spectrum $S_{d1}(\omega)$. Incident wave conditions can be determined by using Equations (26) and (27). Then the first simulation is conducted and the recorded wave spectrum $S_{M1}(\omega)$ can be obtained. In general, $S_{M1}(\omega)$ is not sufficiently close to $S_T(\omega)$; hence, the second simulation should be done similarly. In order to obtain a specified wave spectrum, the driven wave spectrum should be updated by

$$S_{d2}(\omega) = \frac{S_{d1}(\omega)}{S_{M1}(\omega)} S_T(\omega) \tag{28}$$

By using the updated-driven spectrum, the procedures of wave generation and wave simulation mentioned above will be repeated once again and a new recorded wave spectrum can be obtained. After repeating iterated modification and wave simulation one or more times, an accurate approximation time series of the irregular wave can be obtained with an equivalent wave spectrum and wave parameters.

5. MODEL APPLICATIONS AND EXPERIMENTAL VALIDATION

The present meshless NWT is applied to simulate regular and irregular waves. The water depth in the shallow water region is selected as $h_R = 0.26$ m. With a model scale ratio of 1:64, it corresponds to a prototype water depth of 16.7 m. The meshless NWT with the arrangement of collocated boundary points and source points is shown in Figure 4. All the source points are outside the computational fluid domain with the same number as the collocation boundary points. The number of the collocation points on the free surface boundary, the incident boundary, deep water bottom, slope bottom, shallow water bottom and the radiation boundary are $551, 75, 22, 36, 86$ and 10, respectively. The total number is 780.

To validate the model of the meshless NWT, the wave modeling experiment is carried out in the Ocean Engineering Basin in Shanghai Jiao Tong University. The test setup is shown in Figure 5. Four resistance-type wave probes are installed to measure the wave elevations. The No. 1 wave probe is located at the position of $X = 0.5$ m in front of the wave generator, by which the measured wave elevation will be compared with the incident wave in the numerical simulation. The other three wave probes are located at positions of 5, 10 and 15 m in front of the No. 1 wave probe, respectively. The measured wave elevations by the No. 4 wave probe will be considered as the experimental results and compared with the numerical wave elevations.

The wave modeling experiment is conducted according to the procedures in the numerical simulation. The random seed for generating the irregular wave is kept the same in both the computation and the experiment. The incident wave time series in the computation is applied to the driven signals of the physical wave generator, considering the phase difference between a distance of 0.5 m.

Copyright © 2008 John Wiley & Sons, Ltd.

DOI: 10.1002/fld

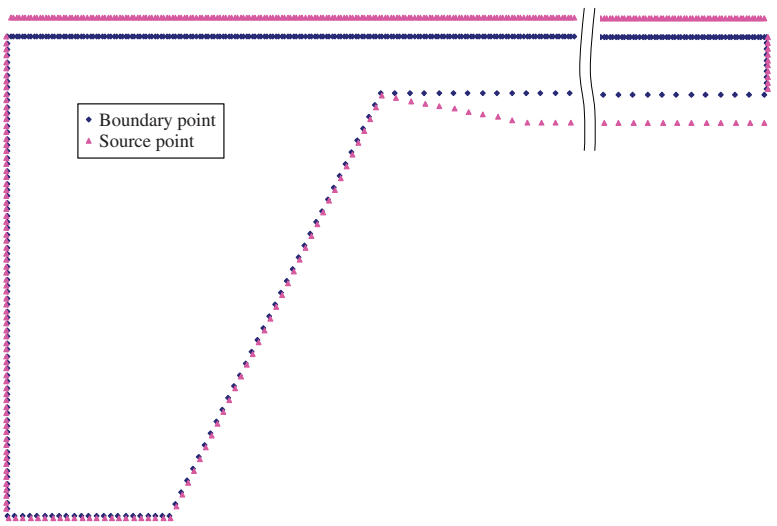

Figure 4. Arrangement of source and boundary points in the meshless NWT.

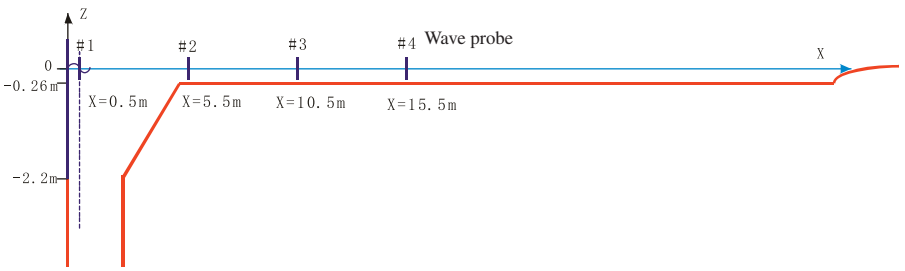

Figure 5. Test setup of wave modeling in the physical ocean engineering basin.

6. RESULTS AND ANALYSES

The present meshless numerical model and NWT are applied to simulate the wave propagation for regular waves and irregular waves in shallow water.

6.1. Simulation of regular waves

Before the simulation of irregular waves, the first application is to simulate the propagation of regular waves. At the incident boundary in deep water, linear regular wave propagating along the x-direction is introduced by the following equations:

$$\eta(x,t)=\frac{H}{2}\cos\theta \tag{29}$$

$$\phi(x,z,t)=\frac{Hg}{2\omega}\frac{\cosh k(z+h)}{\cosh kh}\sin\theta \tag{30}$$

Copyright © 2008 John Wiley & Sons, Ltd.

DOI: 10.1002/fld

where k is the wave number, ω is the circle frequency, H is the wave height, $\theta = kx - \omega t + \pi/2$ denotes the wave phase.

Two regular wave conditions are considered. The wave period, wave height and wavelength for each condition are: (1) $T = 0.6\,\text{s}$, $H = 0.028\,\text{m}$, $\lambda = 0.56\,\text{m}$; (2) $T = 1.29\,\text{s}$, $H = 0.078\,\text{m}$, $\lambda = 2.6\,\text{m}$. In the shallow water region with the water depth of $h_\text{R} = 0.26\,\text{m}$, the first condition also denotes the linear regular wave and the second condition denotes the nonlinear shallow water wave. The wave elevation and the velocity potential can be expressed as the third-order Stokes regular waves as follows:

$$\eta(x,t) = \sum_{m=1}^{3} \eta_m \cos(m\theta) \tag{31}$$

$$\phi(x,z,t) = \sum_{m=1}^{3} \phi_m \sin(m\theta) \tag{32}$$

where

$$\eta_1 = a\left[1 + \frac{k^2a^2}{16}\,\frac{18\cosh^4(kh) - 4\cosh^2(kh) + 1}{\sinh^4(kh)}\right]$$

$$\eta_2 = \frac{ka^2}{4}\,\frac{\cosh(kh)\,[2 + \cosh(2kh)]}{\sinh^3(kh)}$$

$$\eta_3 = \frac{3k^2a^3}{64}\,\frac{1 + 8\cosh^6(kh)}{\sinh^6(kh)}$$

$$\phi_1 = \frac{ac}{\sinh(kh)}\left[1 + \frac{k^2a^2}{16}\,\frac{2 + \cosh(2kh)}{\sinh^4(kh)}\right]\cosh(kz)$$

$$\phi_2 = \frac{3ka^2c}{8\sinh^4(kh)}\cosh(2kz)$$

$$\phi_3 = k^2a^3c\,\frac{11 - 2\cosh(2kh)}{64\sinh^7(kh)}\cosh(3kz)$$

$$H = 2a\left[1 + \frac{k^2a^2}{64}\,\frac{96\cosh^6(kh) - 88\cosh^4(kh) + 20\cosh^2(kh) - 1}{\sinh^6(kh)}\right]$$

The simulation time is $100T$. The modulation time T_m in Equation (13) is chosen as $28T$. The reason for this choice of a long modulation time is to avoid the nonlinear effect of the transient waves in shallow water. The numerical wave profiles in the meshless NWT at the time $40T$ and $100T$ are compared with the analytical solutions, as shown in Figures 6 and 8. The numerical time series of wave elevations at the position of $x = 15\,\text{m}$ and their comparisons with the corresponding analytical solutions are shown in Figures 7 and 9. An obvious phase difference can be observed between the numerical results and the analytical solutions for both the two regular waves. The reason is that the analytical solutions are based on the uniform water depth while the water depth in the present NWT is not uniform. The wave velocity is different. Except for the wave phase,

Copyright © 2008 John Wiley & Sons, Ltd.

DOI: 10.1002/fld

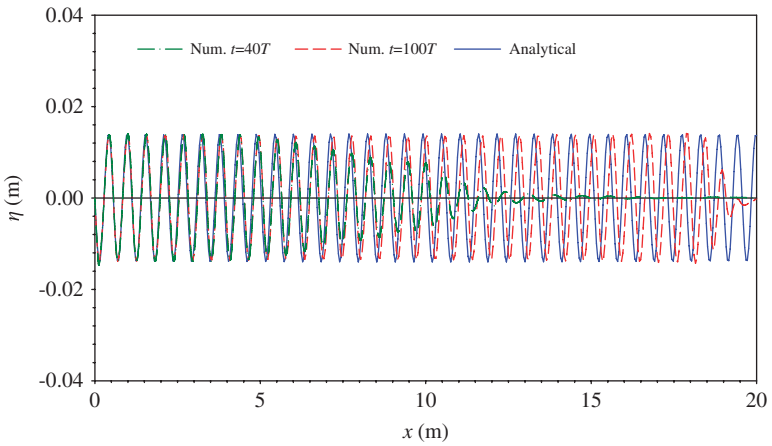

Figure 6. Numerical and analytical wave profiles in the NWT for the case of $T=0.6\,\mathrm{s}$, $H=0.028\,\mathrm{m}$.

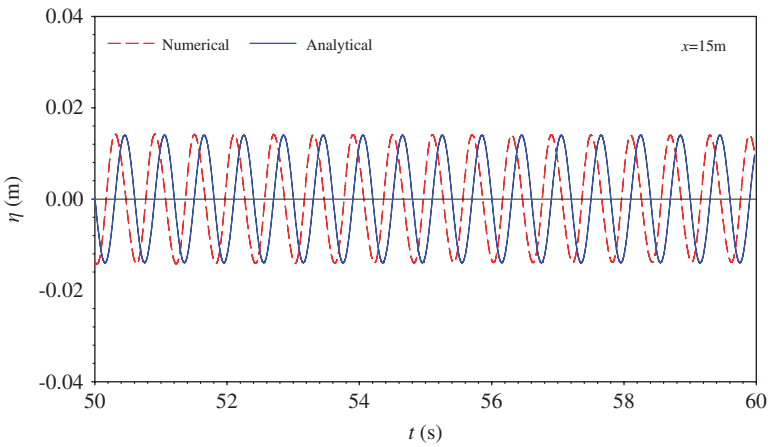

Figure 7. Time series of regular wave at $x=15\,\mathrm{m}$ in shallow water region for the case of $T=0.6\,\mathrm{s}$, $H=0.028\,\mathrm{m}$.

the amplitudes and the profiles of the simulated waves agree well with the analytical solutions. It means that the results will be close to each other if the phase difference is eliminated. The present meshless NWT works well with the given wave propagating problem.

6.2. *Simulation of irregular waves*

The irregular wave spectrum is chosen as JONSWAP spectrum with a peak-enhancement factor of $\gamma=3$. One case with significant wave height $H_s=0.078\,\mathrm{m}$ and peak spectrum period $T_p=1.29\,\mathrm{s}$ is simulated. With a model scale ratio of 1:64, the corresponding prototype values are $H_s=5.0\,\mathrm{m}$ and $T_p=10.3\,\mathrm{s}$, respectively. In the numerical simulation, the time step is selected as $\Delta t=T_p/50$. The total repetition period for the simulation is chosen as $220T_p$, including the modulation time

Copyright © 2008 John Wiley & Sons, Ltd.

DOI: 10.1002/fld

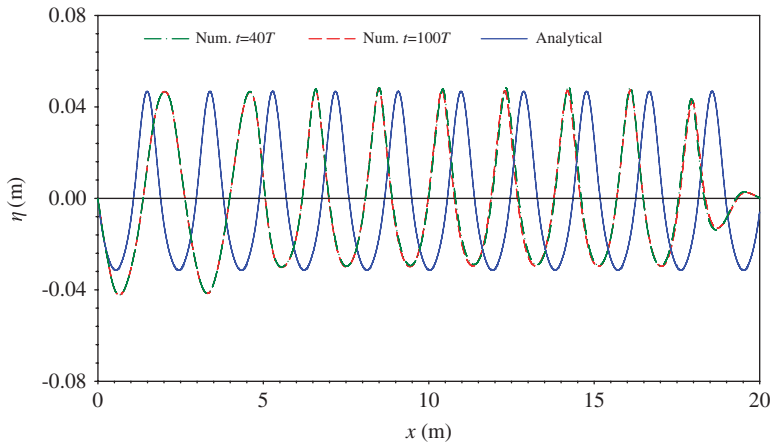

Figure 8. Numerical and analytical wave profiles in the NWT for the case of $T = 1.29\,\mathrm{s}$, $H = 0.78\,\mathrm{m}$.

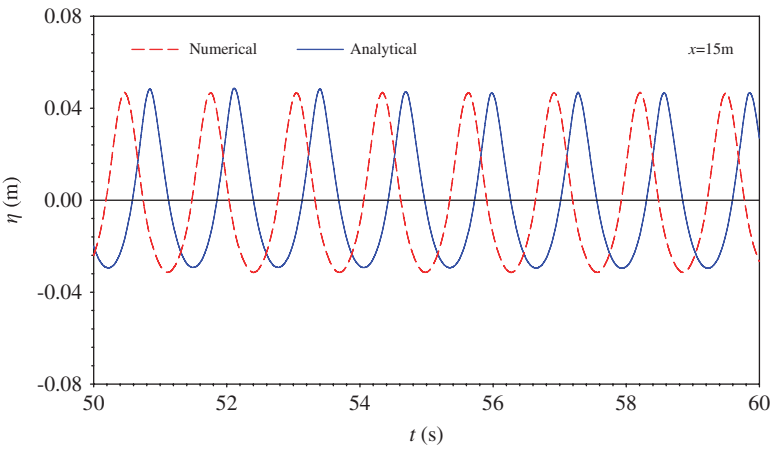

Figure 9. Time series of regular wave at $x = 15\,\mathrm{m}$ in shallow water region for the case of $T = 1.29\,\mathrm{s}$, $H = 0.078\,\mathrm{m}$.

$T_\mathrm{m} = 28T_\mathrm{p}$. Considering the time consumption for the wave propagation from the incident boundary to the radiation boundary, the transient period of the simulated wave elevations at $x = 15\,\mathrm{m}$ should be eliminated and the time series within a range of $45T_\mathrm{p} \sim 209T_\mathrm{p}$ can be utilized to do the subsequent analyses.

First, in order to compare the spectrums of simulated wave elevations with the target spectrum, spectral analysis for the selected time series is carried out by the fast Fourier transform algorithm. In the first simulation, the target wave spectrum $S_\mathrm{T}(\omega)$ is utilized as the driven wave spectrum $S_{\mathrm{d}1}(\omega)$. The time series of the wave elevations recorded by the wave probe located at the position of $x = 15\,\mathrm{m}$ can be obtained and analyzed. Through the spectral analysis, the numerical simulated wave spectrum $S_{\mathrm{M}1}(\omega)$ can be obtained and compared with the target wave spectrum $S_\mathrm{T}(\omega)$ and

Copyright © 2008 John Wiley & Sons, Ltd.

DOI: 10.1002/fld

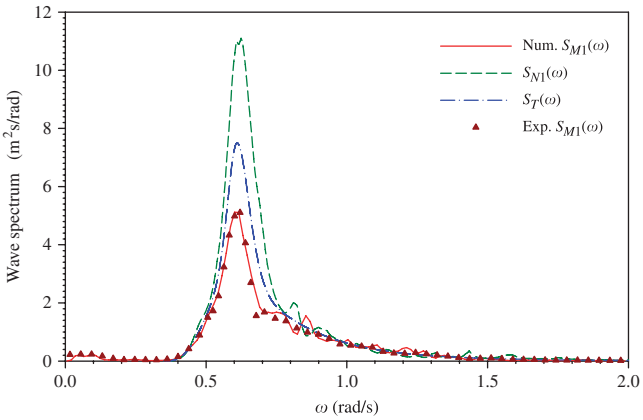

Figure 10. Numerical, experimental, updated and target wave spectrums in the first simulation ($H_s = 5.0\,m$, $T_p = 10.3\,s$).

the corresponding experimental results, as shown in Figure 10. It is shown that the agreement between numerically and experimentally simulated wave spectrums is good but the difference with the target wave spectrum is relatively large. It means the first simulation of the irregular wave doesnot obtain gratifying results and the subsequent iterated modification and simulation should be conducted. The updated wave spectrum $S_{N1}(\omega)$ after the modification by using Equation (28) is also shown in Figure 10.

By using the updated wave spectrum $S_{N1}(\omega)$ as the new driven spectrum $S_{d2}(\omega)$, the second wave generation and wave simulation are conducted numerically and experimentally. A newly simulated wave spectrum $S_{M2}(\omega)$ can be calculated through the spectral analysis and compared with the target wave spectrum $S_T(\omega)$ and the corresponding experimental results, as shown in Figure 11. It is shown that the agreement between not only the numerically and experimentally simulated wave spectrums, but also the simulated wave spectrums and the target one is good.

To validate the simulated irregular waves, not only the wave spectrums but also the main wave parameters should be compared with the target ones. The difference of the simulated and the target significant wave height and peak spectrum period should be less than 5% generally. The main wave parameters in the first and the second numerical and experimental simulation of the irregular wave are analyzed and listed in Table I. It is also shown that the numerical results agree well with the experimental results in each simulation and the final simulated parameters of the irregular wave agree well with the target ones.

In the second simulation, comparisons between the wave elevations at the numerical incident boundary and nearby the physical wave generator are shown in Figure 12. The numerical and experimental time series of the finally simulated irregular wave elevations at $x = 15\,m$ are also shown in Figure 13. A reasonable agreement for both the wave amplitudes and the wave phases is observed between numerical and experimental time series of the wave elevations, except for the initial transition waves. Although the incident waves are linear, the simulated waves in the shallow water region exhibit the characteristics of highly nonlinear waves with steeper wave crests and flatter wave troughs, which are related to nonlinear wave–wave interactions and the shallow water effects. It indicates that the present meshless NWT is valid for the simulation of fully nonlinear

Copyright © 2008 John Wiley & Sons, Ltd.

DOI: 10.1002/fld

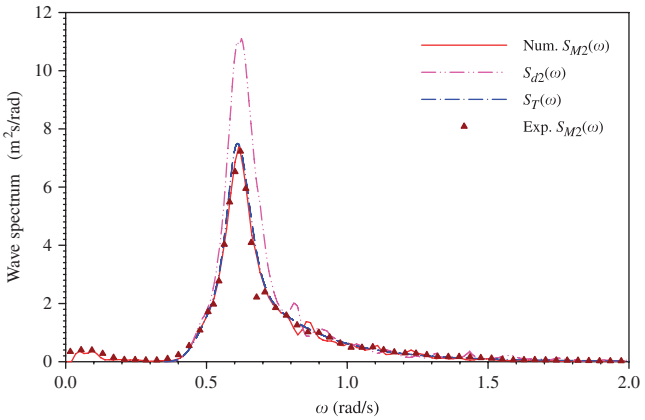

Figure 11. Numerical, experimental, driven and target wave spectrums in the second simulation ($H_s = 5.0$ m, $T_p = 10.3$ s).

Table I. Driven, numerical and experimental parameters of the irregular wave ($H_s = 5.0$ m, $T_p = 10.3$ s).

	Driven spectrum		Numerical results		Experimental results	
Simulation no.	H_s (m)	T_p (s)	H_s (m)	T_p (s)	H_s (m)	T_p (s)
1	5.0	10.3	4.47	10.2	4.40	10.1
2	5.75	10.2	4.92	10.2	4.94	10.1

irregular waves. The simulated time series of the irregular waves can be used as the input of the time domain simulation of the wave-induced motions and forces on floating offshore structures in shallow water.

7. CONCLUSIONS

A NWT similar to the physical ocean engineering basin is developed to simulate the propagation of 2D nonlinear water waves by using the meshless method based on the collocation and the RBF. The fundamental solution of 2D Laplace equation is chosen as the RBF and the source points are placed outside the computational fluid domain. Thus, simple algebraic equations are established and solved directly instead of singular boundary integral equations in traditional BEM. Therefore, an effective numerical model with neither prolix scheme formulation nor time-consuming integration procedure is suitable for simulating nonlinear free surface gravity water wave problems. In order to improve the stability of numerical simulation, the incident boundary condition is given by specifying both the incident wave elevation and velocity potentials. A damping layer combined with the Sommerfeld radiation condition is used as a wave absorber at the radiation boundary. The nonlinear free surface boundary conditions are used for determining the time-stepping integration of wave elevations.

Copyright © 2008 John Wiley & Sons, Ltd.

DOI: 10.1002/fld

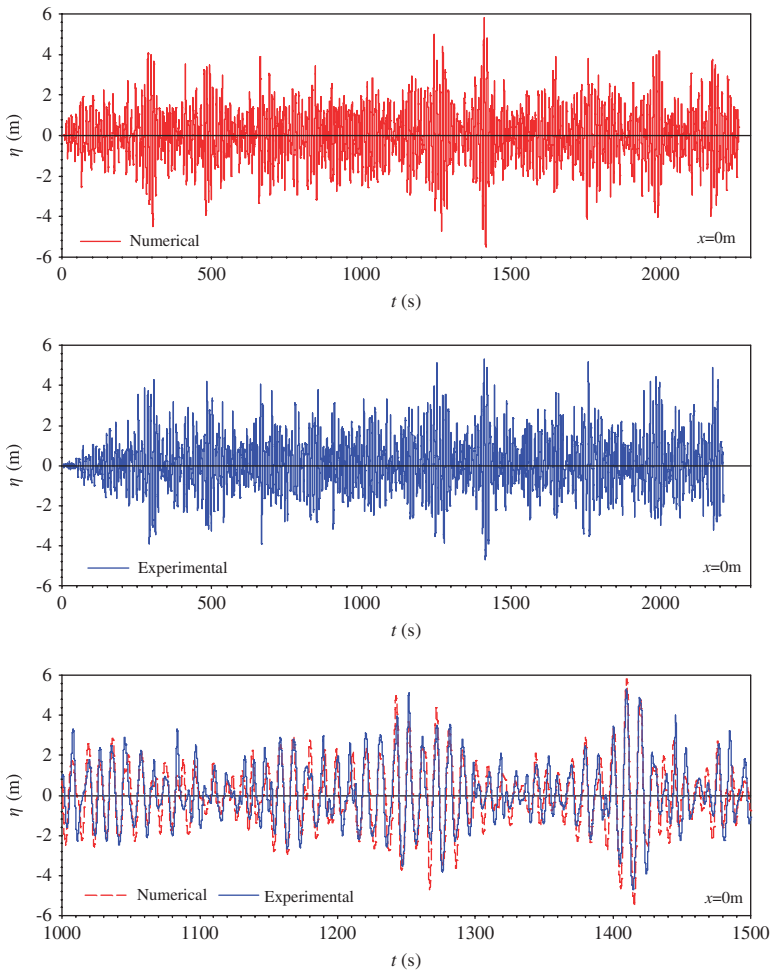

Figure 12. Wave elevations at the numerical incident boundary and nearby the physical wave generator.

In order to simulate the nonlinear irregular waves in shallow water, the shape of the meshless NWT is chosen as the similar profile of the physical ocean engineering basin. The wave will propagate from the deep water region to the shallow water region. Owing to the deep water depth at the incident boundary, the approximation of linear combination of regular wave components is suitable for specifying the incident wave elevation and velocity potentials. Furthermore, an iterated scheme for the modification of the wave spectrum is introduced to simulate specified irregular waves in shallow water.

The present meshless NWT is applied to simulate regular waves and irregular waves in shallow water and validated by analytical solutions and physical experiments. For the simulation of long-time water waves, the meshless NWT is not only easy to be implemented but also economic for the consumption of the CPU time. In the simulation of regular waves, the amplitudes and the profiles of the simulated waves are in reasonable agreement with the analytical solutions. In the

Copyright © 2008 John Wiley & Sons, Ltd.

DOI: 10.1002/fld

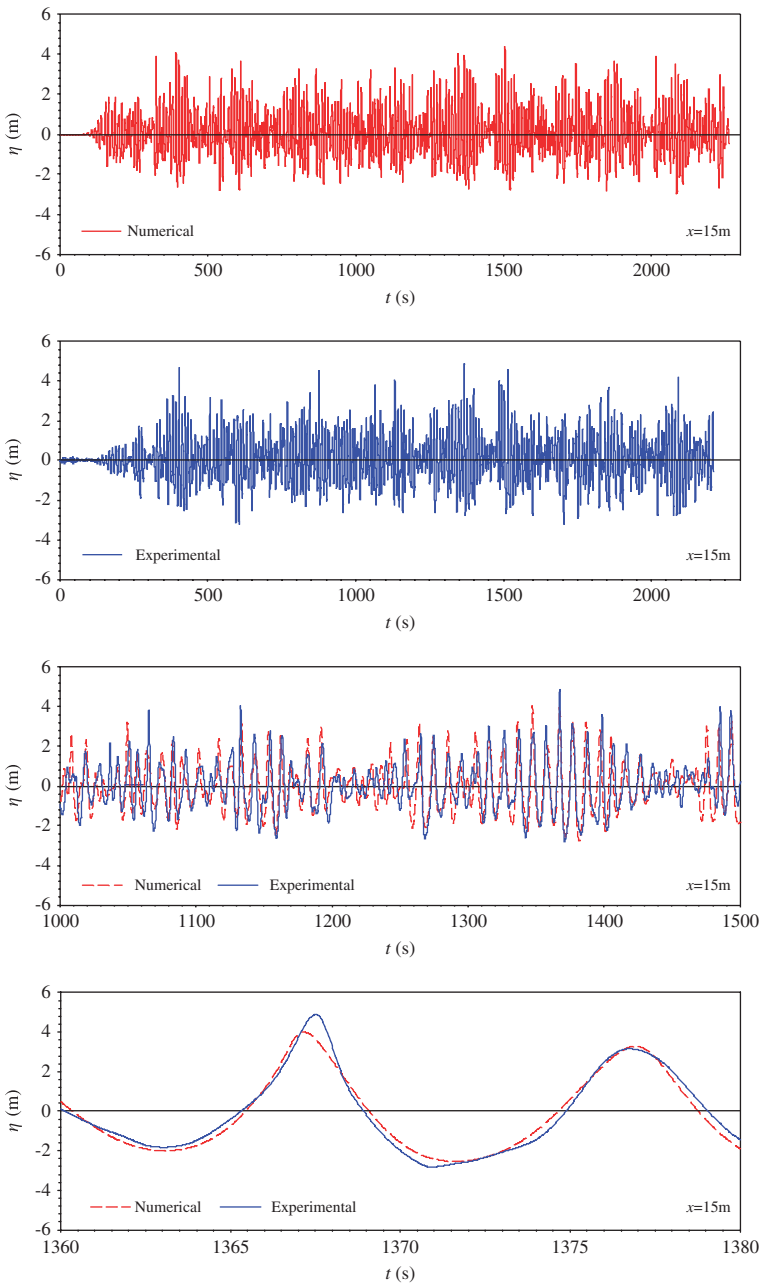

Figure 13. Numerical and experimental time series of irregular waves in shallow water at $x = 15\,\mathrm{m}$.

simulation of irregular waves, the computational wave spectrum, wave parameters and time series match well with the experimental results. The final simulated wave spectrum and wave parameters also match well with the target ones. Although the incident waves are linear, the simulated waves

Copyright © 2008 John Wiley & Sons, Ltd.

DOI: 10.1002/fld

in the shallow water region exhibit the characteristics of nonlinear waves with steeper wave crests and flatter wave troughs, which are related with nonlinear wave–wave interactions and the shallow water effects. It indicates that the present meshless NWT is valid for the simulation of nonlinear irregular waves. The simulated time series of the irregular waves can be used to the time domain simulation of the interaction between offshore structures and irregular waves in shallow water for coastal and ocean engineering applications. However, it remains unclear whether the numerical and experimental solutions correspond to actual ocean waves, which should be studied further if enough observation data of actual ocean waves are available.

ACKNOWLEDGEMENTS

This research work is financially supported by National High Technology and Development Program of China (Grant No. 2006AA09A107) and Shanghai Natural Science Foundation (Grant No. 07ZR14048).

REFERENCES

1. Kim CH, Clement AH, Tanizawa K. Recent research and development of numerical wave tanks—a review. *International Journal of Offshore and Polar Engineering* 1999; **9**(4):241–256.
2. Jamali M. A coupled boundary element-finite difference model of surface wave motion over a wall turbulent flow. *International Journal for Numerical Methods in Fluids* 2006; **51**(4):371–383.
3. Park JC, Kim MH, Miyata H. Fully non-linear free-surface simulations by a 3D viscous numerical wave tank. *International Journal for Numerical Methods in Fluids* 1999; **29**(6):685–703.
4. Bai KJ, Kyoung JH, Kim JW. Numerical computations for a nonlinear free-surface problem in shallow water. *Journal of Offshore Mechanics and Arctic Engineering* 2003; **125**(1):33–40.
5. Ma QW, Wu GX, Taylor RE. Finite element simulation of fully non-linear interaction between vertical cylinders and steep waves. Part 1: Methodology and numerical procedure. *International Journal for Numerical Methods in Fluids* 2001; **36**(3):265–285.
6. Ning DZ, Teng B. Numerical simulation of fully nonlinear irregular wave tank in three dimension. *International Journal for Numerical Methods in Fluids* 2007; **53**(12):1847–1862.
7. Guyenne P, Grilli ST. Numerical study of three-dimensional overturning waves in shallow water. *Journal of Fluid Mechanics* 2006; **547**:361–388.
8. Shih RS, Chou CR, Yim JZ. Numerical investigation on the generation and propagation of irregular waves in a two-dimensional wave tank. *China Ocean Engineering* 2004; **18**(4):551–566.
9. Biausser B, Fraunie P, Grilli ST, Marcer R. Numerical analysis of the internal kinematics and dynamics of 3-D breaking waves on slopes. *International Journal of Offshore and Polar Engineering* 2004; **14**(4):247–256.
10. Hirt CW, Nichols DB. Volume of fluid (VOF) method for the dynamics of free boundaries. *Journal of Computational Physics* 1981; **39**:201–225.
11. Wang P, Yao Y, Tulin MP. An efficient numerical tank for non-linear water waves, based on the multi-subdomain approach with BEM. *International Journal for Numerical Methods in Fluids* 1995; **20**:1315–1336.
12. Longuet-Higgins HS, Cokelet ED. The deformation of steep waves on water. I. A numerical method of computation. *Proceedings of the Royal Society of London* 1976; **A350**:1–26.
13. Rokhlin V. Rapid solution of integral equations of classical potential theory. *Journal of Computational Physics* 1985; **60**:187–207.
14. Nie MX, Wang XM, Li GD, Li LL. Subelement division scheme in a numerical wave tank that uses higher-order boundary element method. *Journal of Waterway, Port, Coastal and Ocean Engineering* 2007; **133**(3):225–229.
15. Hackbusch W, Nowak ZP. On the fast matrix multiplication in the boundary element method by panel clustering. *Numerische Mathematik* 1989; **54**:463–491.
16. Beylkin G, Coifman R, Rokhlin V. Fast wavelet transforms and numerical algorithms I. *Communications on Pure and Applied Mathematics* 1991; **44**:141–183.
17. Roest MRT, Vollebregt EAH, ten Cate HH, Lin HX. Structured parallelization of the flow simulation package TRIWAQ. High-performance computing and networking. *Proceedings of the International Conference and Exhibition*, Milan, 1995; 136–141.

Copyright © 2008 John Wiley & Sons, Ltd.

DOI: 10.1002/fld

18. Madsen PA, Schaffer HA. A review of Boussinesq-type equations for surface gravity waves. *Advances in Coastal and Ocean Engineering*, vol. 5. World Scientific Publishing Co. Pte. Ltd.: Singapore, 1995; 1–95.
19. Gu YT, Liu GR. Meshless methods coupled with other numerical methods. *Tsinghua Science and Technology* 2005; **10**(1):8–15.
20. Atluri SN, Kim HG, Cho JY. A critical assessment of the truly meshless local Petrov–Galerkin (MLPG), and local boundary integral equation (LBIE) methods. *Computational Mechanics* 1999; **24**:348–372.
21. Belytschko T, Lu YY, Gu L. Element-free Galerkin methods. *International Journal for Numerical Methods in Engineering* 1994; **37**:229–256.
22. Liu GR. *Mesh Free Methods*: *Moving Beyond the Finite Element Method*. CRC Press: Boca Raton, U.S.A., 2002.
23. Wang JG, Liu HR. A point interpolation meshless method based on radial basis functions. *International Journal for Numerical Method in Engineering* 2002; **54**:1623–1648.
24. Zhang X, Song KZ, Lu MW, Liu X. Meshless methods based on collocation with radial basis functions. *Computational Mechanics* 2000; **26**(4):333–343.
25. Golberg MA, Chen CS. The method of fundamental solutions for potential; Helmholtz and diffusion problems. *Boundary Integral Methods—Numerical and Mathematical Aspects*. Computational Mechanics Publications: Southampton, Boston, 1998; 103–176.
26. Wu NJ, Tsay TK, Young DL. Meshless numerical simulation for fully nonlinear water waves. *International Journal for Numerical Methods in Fluids* 2006; **50**:219–234.
27. Zhang XT, Kho BC, Lou J. Wave propagation in a fully nonlinear numerical wave tank: a desingularized method. *Ocean Engineering* 2006; **33**:2310–2331.
28. Larsen J, Dancy H. Open boundaries in short wave simulations—a new approach. *Coastal Engineering* 1983; **7**:285–297.
29. Contento G, Codiglia R, D'Este F. Nonlinear effects in 2D transient nonbreaking waves in a closed flume. *Applied Ocean Research* 2001; **23**:3–13.
30. Yu Y, Hong BG, Li YC. A new form of free surface time-stepping for nonlinear wave calculation. *Journal of Dalian Maritime University* 2005; **31**(2):1–3.
31. Zhang YC, Wang MS, Yo MW, Gu QC. Dual flap making wave system and parameterless analysis of wave signal spectrum. *Journal of Shanghai Jiaotong University* 1996; **30**(10):141–146.

Copyright © 2008 John Wiley & Sons, Ltd.

DOI: 10.1002/fld